Engineering with Computers (2010) 26:159–170
DOI 10.1007/s00366-009-0149-y

ORIGINAL ARTICLE

An efficient inverse approach for material hardening parameter identification from a three-point bending test

P.-A. Eggertsen · K. Mattiasson

Received: 19 June 2009 / Accepted: 10 August 2009 / Published online: 10 November 2009

Abstract The cyclic three-point bending test has been frequently used for the determination of material hardening parameters. The advantage of this test is that it is simple to perform, and standard test equipment can be used. The disadvantage is that the material parameter identification requires some kind of inverse approach. The current authors have previously, successfully been utilizing a method, in which computed force–displacement relations have been fitted to corresponding experimental results. The test has been simulated by means of the Finite Element code LS-DYNA, and the material parameters have been determined by finding a best fit to the experimental results by means of the optimization tool LS-OPT, based on a response surface methodology. A problem is, however, that such simulations can be quite time consuming, since the Finite Element model has to be analyzed numerous times. In the current paper, an alternative numerical methodology will be described, in which instead calculated moment–curvature relations are fitted to experimental ones. This optimization procedure does not involve any solution of the FE problem. The Finite Element problem needs only to be solved a limited number of times in an outer iteration loop. This fact results in a considerable reduced computational cost. It is also demonstrated that the parameters determined by this new method correspond excellently to the ones determined by the conventional method.

Keywords Parameter identification · Inverse modeling · Hardening law · Three-point bending · Optimization

P.-A. Eggertsen · K. Mattiasson (✉)
Division of Material and Computational Mechanics,
Department of Applied Mechanics,
Chalmers University of Technology,
412 96 Göteborg, Sweden
e-mail: kjellm@chalmers.se; kmattias@volvocars.com

P.-A. Eggertsen
e-mail: eggepera@chalmers.se

K. Mattiasson
Department 91430, PV22, Volvo Cars Safety Center,
405 31 Göteborg, Sweden

1 Introduction

When a metal sheet is drawn over a die corner, the material is subjected to bending, subsequent unbending, and rebending. In order to perform an accurate simulation of such a sheet metal forming process, it is necessary to have an appropriate constitutive model, which can consider the phenomena that occur during cyclic loading of metal sheets, such as Bauschinger effect, transient behavior, permanent softening, and work-hardening stagnation.

Several purely phenomenological material models have been proposed to describe the cyclic behavior of metal sheets. The complexity of these models varies within a wide range with respect to number of material parameters and history variables. The material parameters involved have to be determined from some kind of cyclic, loading–unloading experiment. In theory, the most simple and straightforward test is a tensile/compression test of a sheet strip. In practice, however, such a test is very difficult to perform, due to the tendency of the strip to buckle in compression. In spite of these difficulties, some successful attempts to perform cyclic tension/compression tests have been reported in the literature; see e.g. Refs. [1–4]. However, common for these tests is that rather complicated test rigs have been designed and used in the experiments, in order to prevent the sheet strip from buckling.

Another kind of tests that frequently have been used for the determination of material hardening parameters is some kind of bending test, see e.g. Refs. [5–8]. The advantage of this kind of tests is that they are simple to perform, and standard test equipments can be used. However, a bending test will involve inhomogeneous stress and strain distributions in the sheet specimen, and the stress–strain relationship cannot be directly determined from the experiment. This means that the material parameters have to be determined by some kind of inverse approach. Usually, the experiments are simulated by FEM, and the material parameters are identified by means of some optimization technique.

A well-established method for physical optimization processes is the response surface methodology (RSM) [9–11]. RSM is a method for replacing a complex and in general unknown model by an approximate one based on results calculated at various points in the design space.

In the present study, a cyclic three-point bending test has been used to identify the material parameters for four different kinematic hardening laws of various complexities, and for four different materials, of which only two are accounted for in the present report. The three-point bending tests were simulated by the Finite Element code LS-DYNA [12]. The inverse methodology for the determination of the material parameters was based on a successive RSM implemented in the optimization code LS-OPT [13]. In the optimization procedure, a calculated cyclic force-deflection response was fitted to a corresponding experimental one.

The drawback of the above procedure is that it can be quite time consuming, especially for more complex hardening laws with many material parameters to be determined. The main reason for the long computing times is the fact that the same FE model has to be analyzed numerous times. In the present paper, an alternative methodology is presented, which can reduce the computing time considerably. The main difference to the "standard" procedure above is that in the new method the moment–curvature at the middle of the sheet strip is studied instead of the force–displacement relationship. The number of times the FE model has to be analyzed can by this methodology be considerably reduced.

2 Constitutive equations

2.1 Introductory remarks

Five different hardening laws were considered in the present study: an isotropic hardening law, a mixed isotropic–kinematic hardening law attributed to Hodge [14] and further developed by Crisfield [15], the Armstrong–Frederick hardening law [16], the Geng–Wagoner hardening law [17], and, finally, the Yoshida–Uemori hardening law [18]. All these criteria are implemented by the authors in the finite element code LS-DYNA [12] together with the eight parameter yield criterion by Banabic and Aretz [19, 20]:

$$\bar{\sigma} = \left[\frac{1}{2}\left(|\Gamma+\Psi|^M+|\Gamma-\Psi|^M+|2\Lambda|^M\right)\right]^{\frac{1}{M}} \tag{1}$$

The functions Γ, Ψ and Λ are defined as

$$\begin{aligned}\Gamma &= \frac{L\sigma_{xx}+K\sigma_{yy}}{2}\\ \Psi &= \sqrt{\frac{\left(N\sigma_{xx}-P\sigma_{yy}\right)^2}{4}+Q^2\sigma_{xy}\sigma_{xy}}\\ \Lambda &= \sqrt{\frac{\left(R\sigma_{xx}-S\sigma_{yy}\right)^2}{4}+T^2\sigma_{xy}\sigma_{xy}}\end{aligned} \tag{2}$$

where the parameters L, K, N, P, Q, R, S, and T are identified from uniaxial and bulge test data.

Below follows a brief description of the four kinematic hardening models used in the current study. For a detailed description of these hardening laws, the reader is referred to a recent paper by the authors Eggertsen and Mattiasson [21].

2.2 Mixed hardening

The hardening law that is called "mixed hardening" in this study is a combination of isotropic and kinematic hardening, where the proportion of isotropic and kinematic hardening is weighted with a scalar m. The scalar m represents the ratio of plastic strain associated to isotropic hardening, whereas the ratio $(1-m)$ is left for the kinematic hardening response. From this, it follows that:

$$\begin{aligned}&\dot{\boldsymbol{\varepsilon}}^p = \dot{\boldsymbol{\varepsilon}}^p_{\text{iso}}+\dot{\boldsymbol{\varepsilon}}^p_{\text{kin}} = m\dot{\boldsymbol{\varepsilon}}^p+(1-m)\dot{\boldsymbol{\varepsilon}}^p\\ &0\le m\le 1\end{aligned} \tag{3}$$

The evolution of the back-stress $\boldsymbol{\alpha}$ can then be expressed as

$$\dot{\boldsymbol{\alpha}} = \left(H'-\tilde{H}'m\right)\frac{\dot{\bar{\varepsilon}}^p}{\bar{\sigma}}(\boldsymbol{\sigma}-\boldsymbol{\alpha}) \tag{4}$$

where H' is the slope of the plastic hardening curve at the strain level $\bar{\varepsilon}^p$ and $\tilde{H}'$ is the slope at $\bar{\varepsilon}^p_{\text{iso}} = m\bar{\varepsilon}^p$.

The mixed hardening law is able to consider the Bauschinger effect and the permanent softening behavior.

2.3 Armstrong–Frederick hardening

The second hardening law is the well-known one by Armstrong and Frederick [16], who prescribed the back-stress evolution according to:

$$\dot{\boldsymbol{\alpha}} = C_x \left[\alpha_{\text{sat}} \frac{\boldsymbol{\sigma} - \boldsymbol{\alpha}}{\bar{\sigma}} - \boldsymbol{\alpha} \right] \dot{\bar{\varepsilon}}^p \tag{5}$$

where α_{sat} and C_x are material parameters. The Armstrong–Frederick hardening law is able to consider the Bauschinger effect and the transient behavior.

2.4 Geng–Wagoner hardening

The Geng–Wagoner hardening law is an extension of the Armstrong–Frederick law, and involves two surfaces: a yield surface and a bounding surface. The Geng–Wagoner law includes translation of the bounding surface, in order to capture the permanent softening effect. The evolution equations are as follows

$$\dot{\boldsymbol{\alpha}} = C_x \left[\frac{\alpha_{\text{sat}}}{\bar{\sigma}} (\boldsymbol{\sigma} - \boldsymbol{\alpha}) - (\boldsymbol{\alpha} - \boldsymbol{\beta}) \right] \dot{\bar{\varepsilon}}^p \tag{6}$$

$$\dot{\boldsymbol{\beta}} = \frac{H' - \tilde{H}' m}{\bar{\sigma}} (\boldsymbol{\sigma} - \boldsymbol{\alpha}) \dot{\bar{\varepsilon}}^p \tag{7}$$

where $\boldsymbol{\alpha}$ is the center of the yield surface and $\boldsymbol{\beta}$ is the center of the bounding surface. As can be seen from Eq. 7, the hardening of the bounding surface is governed by the mixed hardening law (Eq. 4). The Geng–Wagoner hardening law can consider the early re-yielding, the transient behavior and the permanent softening effect.

2.5 Yoshida–Uemori hardening

The final hardening law is the one by Yoshida and Uemori. The model includes both translation and expansion of the bounding surface, while the active yield surface only evolves kinematically. The evolution of the back-stress is expressed as

$$\dot{\boldsymbol{\alpha}} = \dot{\boldsymbol{\alpha}}^* + \dot{\boldsymbol{\beta}} \tag{8}$$

with

$$\dot{\boldsymbol{\alpha}}^* = C_x \cdot \left(\frac{B + R - Y}{Y} \cdot (\boldsymbol{\sigma} - \boldsymbol{\alpha}) - \boldsymbol{\alpha}^* \right) \cdot \dot{\bar{\varepsilon}}^p$$

$$\dot{\boldsymbol{\beta}} = k \cdot \left(\frac{b}{B + R} \cdot (\boldsymbol{\sigma} - \boldsymbol{\beta}) - \boldsymbol{\beta} \right) \cdot \dot{\bar{\varepsilon}}^p$$

where $\boldsymbol{\alpha}^*$ is the relative kinematic motion of the yield surface with respect to the bounding surface, $\boldsymbol{\beta}$ is the center of the bounding surface, B is the initial size of the bounding surface, Y is the size of the yield surface, C_x and k are material parameters, and R, finally, is the isotropic hardening of the bounding surface:

$$\dot{R}(\bar{\varepsilon}^p) = k(R_{\text{sat}} - R(\bar{\varepsilon}^p)) \dot{\bar{\varepsilon}}^p \tag{10}$$

In Eq. 10, R_{sat} is a material parameter describing the upper limit of isotropic hardening. In the current work, a slightly modified version of this hardening law is used, in which only the parameters C_x, k, b, and h are employed. For a detailed description of the current implementation, see Eggertsen and Mattiasson [21]. The Yoshida–Uemori hardening law considers all the effects presented in Fig. 1.

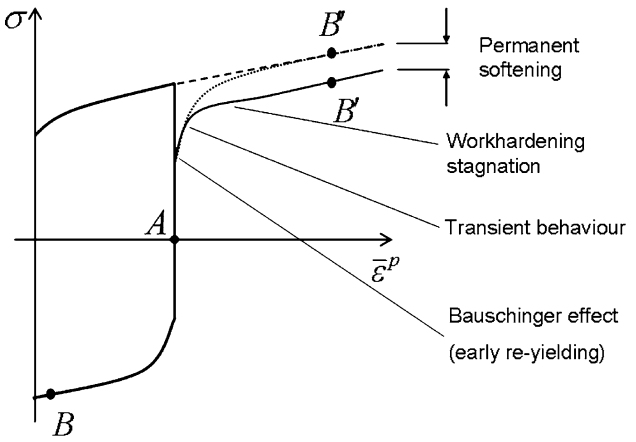

Fig. 1 Schematic unloading curve to illustrate the Bauschinger effect, the transient behavior, the permanent softening behavior, and the work-hardening stagnation

Table 1 Number of material hardening parameters and history variables in the hardening models studied in the present work

Hardening model	Number of material hardening parameters	Number of history variables
Isotropic	0	1
Mixed	1	4
Armstrong–Frederick	2	4
Geng–Wagoner	3	7
Yoshida–Uemori	4	10

2.6 Number of material parameters and history variables: a summary

The number of material hardening parameters and history variables for the hardening models described above is summarized in Table 1. Especially, the number of hardening parameters is important in the present context, since it has a great impact on the computing time needed for determining the parameters in the optimization procedure.

3 Materials

Two different steel grades are considered in the current report: a DP600-steel and a 220IF-steel. To determine the parameters for the yield criterion discussed in Sect. 2.1, yield stresses and Lankford parameters (r values) for the rolling, transverse and diagonal directions, respectively,

Table 2 Mechanical properties for the steel grades included in the current report

Material	σ_0 (MPa)	σ_{45} (MPa)	σ_{90} (MPa)	σ_b (MPa)	r_0	r_{45}	r_{90}	r_b	Thickness (mm)
TKS-DP600HF	363.70	382.60	401.20	374.70	0.46	0.88	1.00	0.85	1.46
TKS-220IF	226.70	238.90	246.40	276.98	1.60	2.10	2.42	0.96	0.96

were determined. These values were obtained from simple uniaxial tension tests in the directions of interest. The uniaxial tests were complemented with viscous bulging tests, aiming at providing plastic hardening data for strain levels much higher than what can be achieved in ordinary tensile tests and providing data for the equibiaxial yield stress σ_b and r-value r_b. The yield stresses, r values and thicknesses for the two materials are listed in Table 2.

4 Three-point bending test

4.1 Experimental set-up

The cyclic three-point bending test is a relatively simple and convenient experiment for determining the kinematic hardening parameters for sheet metals. The test has been suggested in the literature by, e.g., Zhao and Lee [5]. The equipment used in the current experiments has previously been described in Omerspahic et al. [6] and Eggertsen and Mattiasson [21]. The test set-up is illustrated in Fig. 2. Especially, the design of the end supports should be noticed. These provide a moment-free support, while the sheet strip is allowed to slip freely between two rollers in the axial direction. The punch in the middle is moved with a prescribed sinusoidal displacement. The distance between the end supports is 100 mm, and the width of the sheet strip is 20 mm for the 220IF material and 25 mm for the DP600 material. The punch force is measured by means of a load cell. During the test, the punch force and punch displacement are recorded. The error in displacement reading is estimated to ±0.02 mm and in force reading ±3 N.

The maximum strain level reached in this test is about 5%. This is a lower level than what is achieved in many practical cases. On the other hand, the same set of hardening parameters has to be assumed to be applicable for all strain levels.

4.2 FE model

In the inverse approach for determining the hardening parameters, the bending test was simulated by means of the explicit FE code LS-DYNA [12]. One quarter of the sheet strip was modeled with triangular shell elements. Convergent results were obtained with 160 elements and 9 integration points through the thickness. The triangular shell element used here is the linear, Mindlin one by Kennedy et al. [22]. The FE model is shown in Fig. 3. Special care has been devoted to a correct modeling of the end supports. Just as for the experimental set-up, the support is free to rotate around its own axis. The support was modeled with two rigid plates with a frictionless contact to the specimen, such that the sheet material can slip freely in the longitudinal direction.

5 Optimization algorithm

5.1 The response surface methodology

The inverse procedure used to determine the material hardening parameters was based on a RSM and the optimization software LS-OPT [13]. RSM is a mathematical method for constructing smooth approximations of

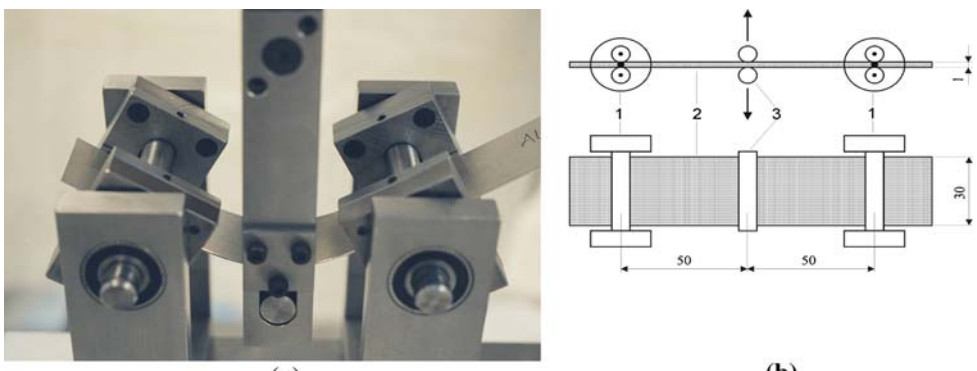

Fig. 2 Experimental set-up used in the three-point cyclic bending tests: **a** a picture of the experimental equipment; **b** a sketch of the test arrangement

Fig. 3 FE model of the three-point bending test

complex functions in a design space. The approximations are based on numerous points in the multi-dimensional design space, and they are most often based on low-order polynomial functions for simplicity. The response surface is fitted to the points in the design space using regression analysis, usually least square approximations.

Thus, the experimental points construct an approximate design space wherein an objective function can be optimized. The choice of locations of the points in the design space, the *experimental design* or *design of experiments* (DOE), is done in a, in some meaning, optimal way. There are several experimental design criteria available in LS-OPT. We have in this study chosen the so-called *D-optimality* criterion, which is the default method in LS-OPT.

Generally, a high-order polynomial approximation yields a better accuracy and faster convergence toward an optimum than a low-order approximation. On the other hand, a high-order approximation requires more points (more function evaluations) in the design space, and thereby more computing time. In the current study, a second-order polynomial approximation has been found to be an optimal choice.

In LS-OPT a so-called *sequential response surface method* (SRSM) is used. In SRSM, a subspace of the design space, a *region of interest*, is used to determine an approximate optimum. A region of interest is based on assumed limits of the design variables. A new region of interest is prescribed for each new iterative step in the optimization process by reducing its size (zooming), and centering it around the last calculated optimum point (panning). A schematic illustration of the pan and zoom procedure is shown in Fig. 4.

The necessary number of experimental points is decided by the number of design parameters, the choice of polynomial approximation, and the chosen experimental design criterion. The number of required experimental design points for the D-optimality criterion is listed in Table 3 for first- and second-order polynomial approximations.

The various steps in the optimization procedure, during a single iteration, can, thus, be summarized as follows:

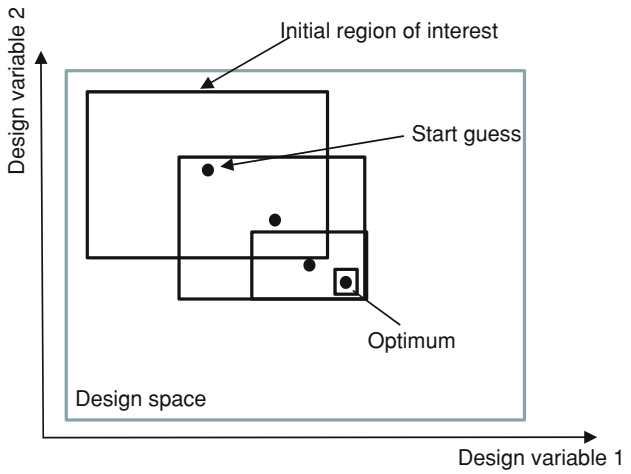

Fig. 4 Schematic illustration of the pan and zoom method for the case of two design variables

- Define, in some meaning, an optimal choice of points in the design space (*DOE*).
- Calculate the *objective function* in all points.
- Fit a polynomial surface to the calculated points (*response surface*).
- Calculate the minimum point on the response surface by means of some kind of gradient-based optimization procedure.
- Define a new *region of interest* (*panning and zooming*).
- Return to step 1 and continue until convergence.

5.2 User-defined parameters

There are, thus, a number of parameters, which the user has to select, and which he must be aware of can influence both the efficiency of the optimization procedure as well as the result of it. Following is a list of such parameters:

- The order of the polynomial approximation (here, second order).
- Choice of DOE (here, the *D-optimality* criterion).
- Initial limits of the design variables (initial *region of interest*).
- Start values for the design variables.

Table 3 Number of experimental points required for experimental designs for linear and quadratic approximations, respectively

Number of variables	Linear approx.	Quadratic approx.
1	4	5
2	5	10
3	7	16
4	8	23
5	10	32

6 Procedures for material parameter identification from the three-point bending test

6.1 Standard identification procedure

In the previously used identification procedure, here called the "standard" procedure, for hardening parameter identification, simulated and experimental punch forces were compared, and the corresponding mean squared error (MSE) was calculated. In LS-OPT, the MSE is defined as

$$\varepsilon = \frac{1}{P}\sum_{p=1}^{P} W_p \left(\frac{f_p(\mathbf{x}) - G_p}{s_p}\right)^2 = \frac{1}{P}\sum_{p=1}^{P} W_p \left(\frac{e_p(\mathbf{x})}{s_p}\right)^2 \qquad (11)$$

where $f_p(\mathbf{x})$ are the values on the computed curve, G_p are the values on the target curve, $\mathbf{x}$ is a vector with design variables, s_p are residual scale factors, and W_p are weights applied to the square of the scaled residual $(f_p - G_p)/s_p$ at point p. For all variables, the index p is running from 1 to P. That is, the smaller error, the better fit to the experimental data. In this work, all parts of the target curve are considered to be of equal importance, and the weight and scale factors are therefore set to 1.

With this in mind, Eq. 11 can be rewritten as

$$\varepsilon(\mathbf{p}) = \frac{1}{P}\sum_{p=1}^{P} \left(f_p(\mathbf{p}) - G_p\right)^2 \qquad (12)$$

where $f_p(\mathbf{p})$ are the predicted punch forces, G_p are the corresponding values from the experimental three-point bending test, and $\mathbf{p}$ is a vector with material hardening parameters. The MSE function given by Eq. 12 is considered as the objective function in the design space, defined by

$$p_i^{\min} \le p_i \le p_i^{\max} \quad i = 1, 2, \ldots, n \qquad (13)$$

where $p_i^{\min}$ and $p_i^{\max}$ represent the lower and the upper limits, respectively, of the design variable p_i, and n is the number of unknown material parameters.

A scheme for the standard identification model is presented in Fig. 5. Based on an initial guess, the LS-OPT software prepares N input decks for the FE simulations, where N is the number of experimental design points needed for building the design space described in Table 3. Each input deck has different material parameter set-ups inside the design space. Each FE simulation is run, and the predicted punch forces are compared to the experimental punch forces, and the MSEs are calculated according to Eq. 12. Based on the MSE values, the LS-OPT software calculates an optimal parameter set-up by means of the RSM. If a converged solution is not found, the process starts all over again, but with a new region of interest in the design space.

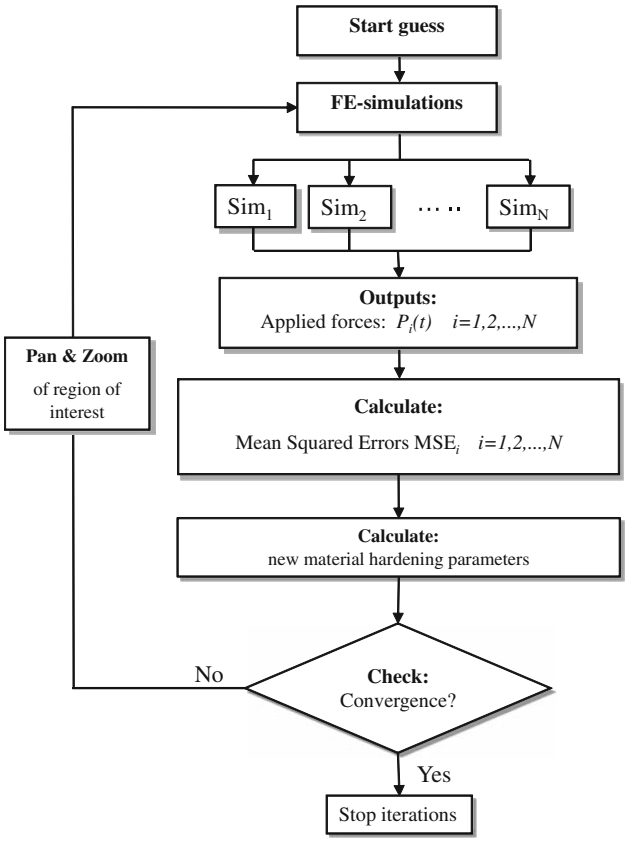

Fig. 5 Scheme for the standard identification procedure

For building the design space, the FE model presented earlier in Sect. 4.2 has been analyzed between 5 and 23 times in each iteration step depending on the current hardening model (see Table 3). For the hardening model with one single hardening parameter (mixed hardening), a total of 25–40 function evaluations were needed, while the model with four hardening parameters (Yoshida–Uemori) required 150–200 function evaluations. Obviously, this is a very CPU time consuming procedure, and in order to reduce the computational effort, an alternative and more efficient identification procedure has been developed. This method is presented in the next section.

6.2 Modified identification procedure

As described in the previous section, a large number of solutions of the FE problem are needed in the "standard" methodology, leading to an extensive computing time. In order to reduce the total CPU time, a more effective identification procedure is presented below.

Instead of using the punch force, the bending moment at the center cross-section of the sheet strip can be used as a target value in the MSE criterion. Equation 12 can then be rewritten as

$$\varepsilon(\mathbf{p}) = \frac{1}{P}\sum_{p=1}^{P}\left(M_p^c(\mathbf{p}) - M_p^t\right)^2 \tag{14}$$

where $M_p^c(\mathbf{p})$ represent the calculated bending moments as a function of the unknown material parameter vector $\mathbf{p}$, and M_p^t represent the target bending moments. The MSE function given by Eq. 14 is now considered as the objective function in the design space defined according to Eq. 13.

A simple equilibrium equation around the mid-section of the sheet strip yields the target moment according to (see Fig. 6):

$$M^t = \frac{P}{2}L + F_x u_z \tag{15}$$

where L is the length between the bearing and the applied punch load, u_z is the vertical prescribed displacement of the punch, P is the punch force, and F_x, finally, is the horizontal reaction force.

In the calculation of the bending moments $M^c(\mathbf{p})$, it is assumed that the strains are linearly distributed through the thickness. Based on this assumption, the bending moment about the sheet centerline is determined by integration of the tangential stresses over the thickness such that:

$$M^c(\mathbf{p}) = w\int_{-t/2}^{t/2}\sigma_x(\mathbf{p},z)z\,dz \tag{16}$$

where t and w are the sheet thickness and sheet width, respectively, and z represents the through thickness coordinate.

The calculation of the strains through the thickness presupposes that the curvature κ of the mid-section is known. The stresses can then be calculated from the known strains through the constitutive relation, which involves the hardening law. These calculation steps are schematically illustrated in Eq. 17:

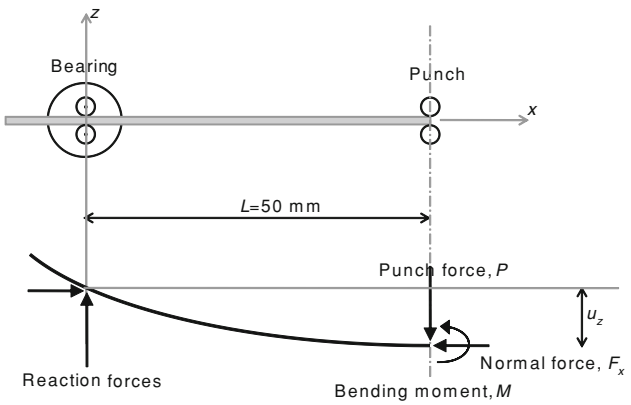

Fig. 6 Acting forces on one half of the sheet strip

$$\kappa \xrightarrow{z} \varepsilon_x(z) \xrightarrow{\text{constitutive relation}} \sigma_x(\mathbf{p},z) \tag{17}$$

There are, however, two problems in connection to the calculation scheme described by Eqs. 15–17. These problems are that neither the force F_x in Eq. 15 nor the curvature κ in Eq. 17 is a known quantity from the experiment.

To circumvent these problems in the identification procedure for the hardening parameters, the calculations are performed in two nested iteration loops. In the outer loop (see Fig. 8), the FE problem is solved once for the last calculated set of hardening parameters. As outputs from the FE simulation, the force F_x and the strains at the extreme layers of the mid-section are recorded. From these strains, the curvature of the mid-section can be easily calculated.

Knowing these quantities, it is now possible to enter the inner iteration loop (see Fig. 9), which is basically identical with the calculation scheme for the standard method described in Fig. 5, with the difference that the MSEs now are calculated based on the mid-section moments according to Eq. 14. An illustration of a typical moment–curvature curve used as target curve in the optimization routine can be seen in Fig. 7.

The calculations proceed until convergence is reached in the outer iteration loop for the extreme layer strains in the mid-section. With this procedure, the total number of required FE analyses is limited to 8–10. This results in a drastic reduction of computing time compared to the standard procedure for hardening parameter identification.

6.3 Performances of the identification procedures

The performances of the two models were evaluated based on two criteria: the MSE value and the total CPU time. The MSE value is an indicator of the accuracy of the material model with the obtained material parameters (the lower MSE value, the better accuracy).

It should be noted that the CPU time is strongly dependent on the starting guess, and the values presented in this report are based on an arbitrary, but reasonable initial guess. Furthermore, it should be mentioned that the CPU

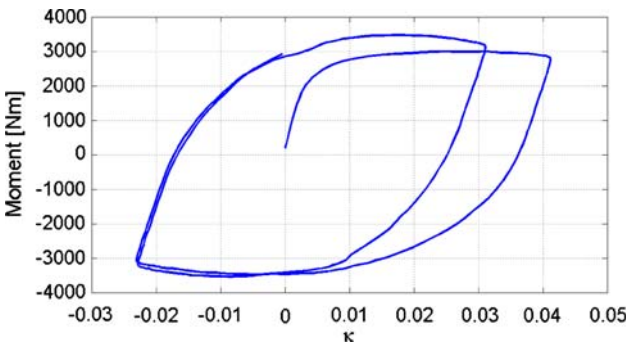

Fig. 7 Illustration of a typical moment–curvature curve used as target curve in the optimization procedure for the new approach

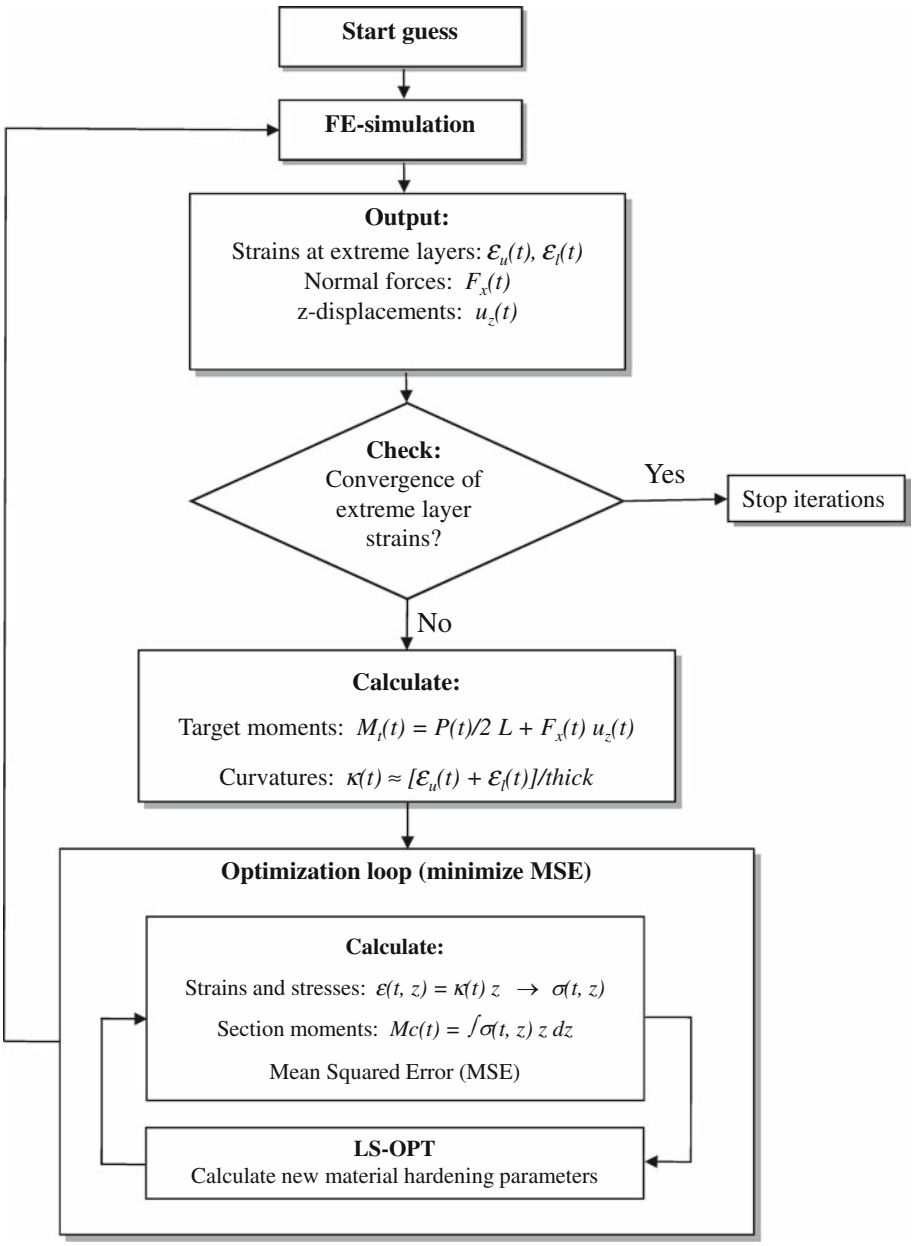

Fig. 8 Scheme for the modified parameter identification method

times indicated in the tables below are the time to run the problem on one, single processor. For the basic identification procedure, there is a possibility to perform the calculations on several parallel processors. For instance, for the Armstrong–Frederick hardening law, with two material parameters, it is possible to perform ten simulations at the same time. This means that the real time (clock time) for the identification procedure can be reduced substantially.

The CPU times and the MSEs for the two methods and for the two materials are presented in Tables 4 and 5. The tables clearly show that the two methods yield more or less the same results in terms of MSE value. However, the total CPU time is much lower for the modified method. This is due to the fact that the total number of FE simulations is heavily reduced for the modified method. The total number of FE simulations can also be seen in Tables 4 and 5. However, it should be mentioned that the new method leads to an increased number of total optimization loops, since a whole optimization has to be performed after each FE simulation (the inner loop illustrated in Fig. 9). However, this optimization procedure is fast and only takes a few minutes. The total number of optimization iterations needed inside this inner loop is dependent on the number of unknown parameters, and of the quality of the parameter set-up used in the FE simulation. In Figs. 10 and 11, the resulting force–displacement curves for the four hardening models are compared with experimental curves.

Table 4 Obtained MSEs, CPU times and total number of FE simulations for the standard and the modified identification procedures for the TKS-DP600 material

Hardening model	Standard identification method			Modified identification method		
	MSE	CPU time (h)	No. of FE-sim	MSE	CPU time (h)	No. of FE-sim
Mixed hardening	0.09105	6.0	30	0.09096	2.0	4
Armstrong–Frederick	0.00463	16.8	70	0.00456	2.8	5
Geng–Wagoner	0.00213	26.4	96	0.00219	4.0	8
Yoshida–Uemori	0.00168	75.0	230	0.00171	8.0	13

Table 5 Obtained MSEs, CPU times and total number of FE simulations for the standard and the modified identification procedures for the TKS-220IF material

Hardening model	Standard identification method			Modified identification method		
	MSE	CPU time (h)	No. of FE-sim	MSE	CPU time (h)	No. of FE-sim
Mixed hardening	0.09853	8.0	30	0.09804	2.2	5
Armstrong–Frederick	0.08605	18.6	70	0.08621	3.0	6
Geng–Wagoner	0.07653	23.2	96	0.07598	4.3	8
Yoshida–Uemori	0.07186	82.5	262	0.07164	9.0	14

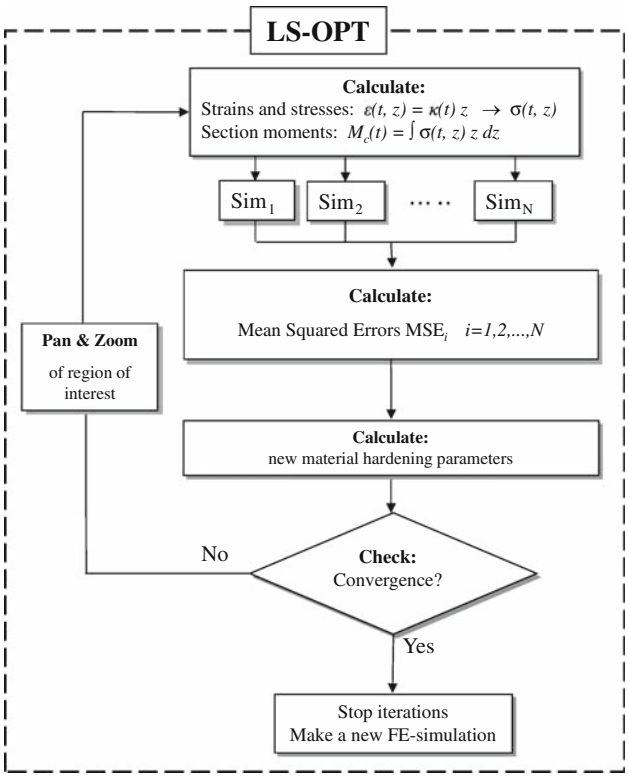

Fig. 9 Scheme for the LS-OPT part in Fig. 8

It should, finally, be mentioned that for some cases, there exist several optimal solutions that give more or less the same MSE value. This is especially evident for the Yoshida–Uemori model that involves four unknown material parameters. Both the standard and the modified procedure are able to find these different optimal solutions. Which optimum that is found depends on the initial starting guess. However, based on the same initial guess, the two methods do not necessarily end up with the same optimal solution.

7 Conclusions

The cyclic three-point bending test has been used to determine the material parameters for various hardening laws. Two different inverse approaches have been used, in which the test has been simulated by means of the FE code LS-DYNA. A response surface method and the optimization code LS-OPT have been used to determine the optimal material parameters.

In the original inverse identification methodology, the parameters were determined to give an optimal fit to the measured force–displacement curve. This procedure, however, is quite time consuming, since numerous FE simulations have to be performed.

In the current paper, an alternative procedure is proposed, in which the calculated moment–curvature curve is fitted to the corresponding measured one. This optimization procedure does not involve any solution of the FE problem. The Finite Element problem needs only to be solved a limited number of times in an outer iteration loop. It has been demonstrated that this procedure offers considerable advantages in terms of computing time. It has also been shown that the parameters determined by this new method correspond excellently to the ones determined by the conventional method.

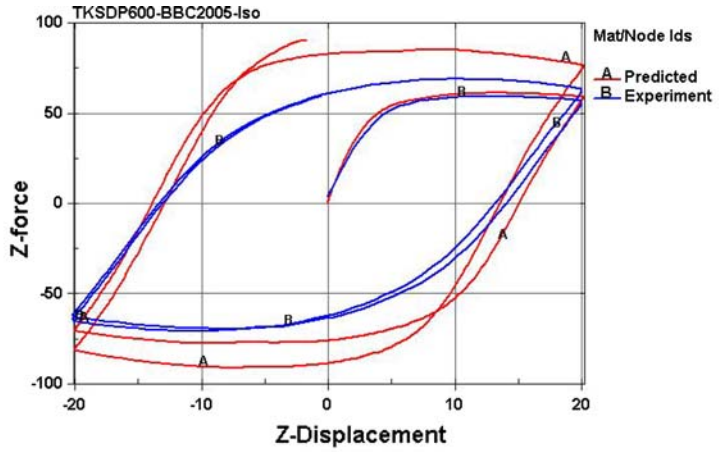

(a) Isotropic hardening

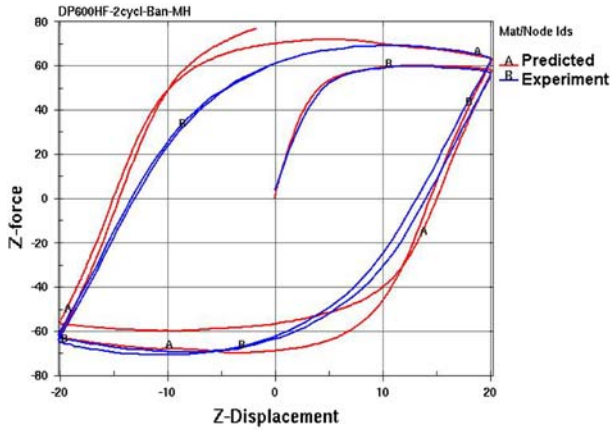

(b) Mixed hardening

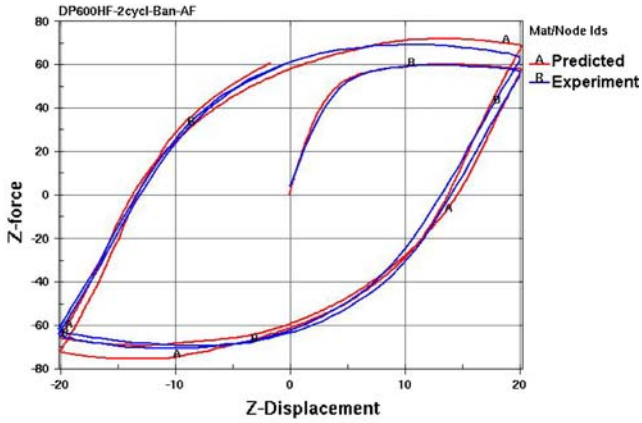

(c) Armstrong-Frederick hardening

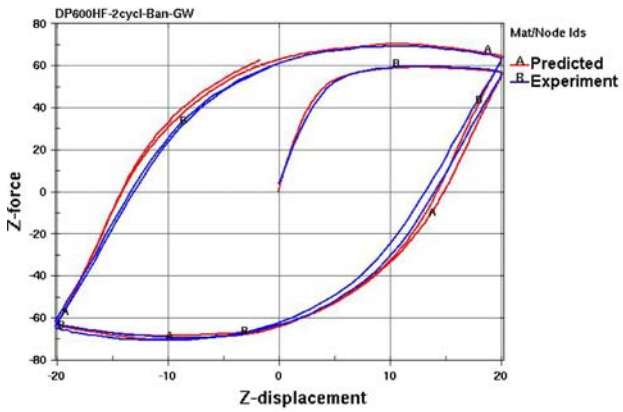

(d) Geng-Wagoner hardening

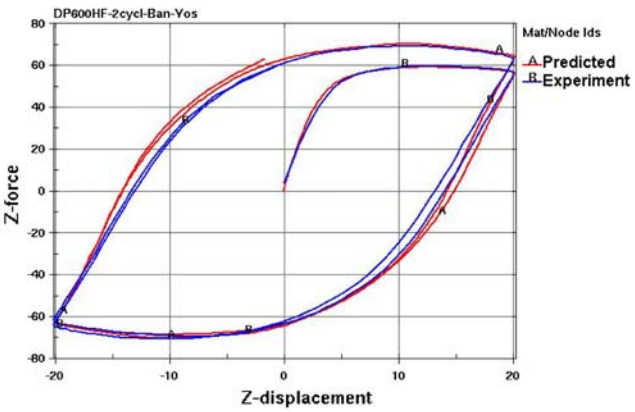

(e) Yoshida-Uemori hardening

Fig. 10 Fitting of simulated three-point bending tests to experimental results using the modified identification procedure and the five different hardening laws (two cycles). Material: TKS-DP600

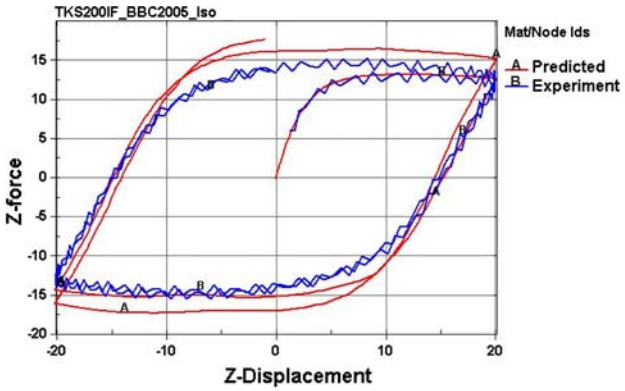

(a) Isotropic hardening

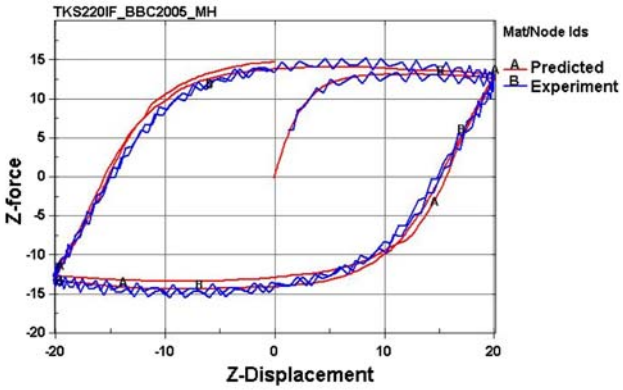

(b) Mixed hardening

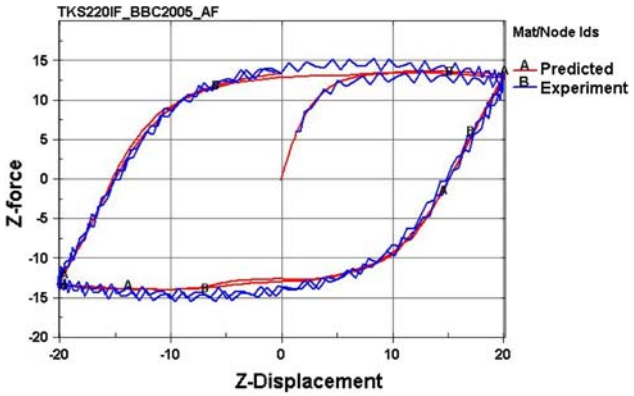

(c) Armstrong-Frederick hardening

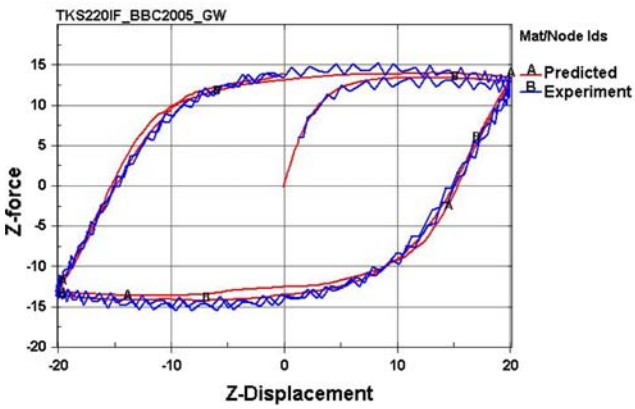

(d) Geng-Wagoner hardening

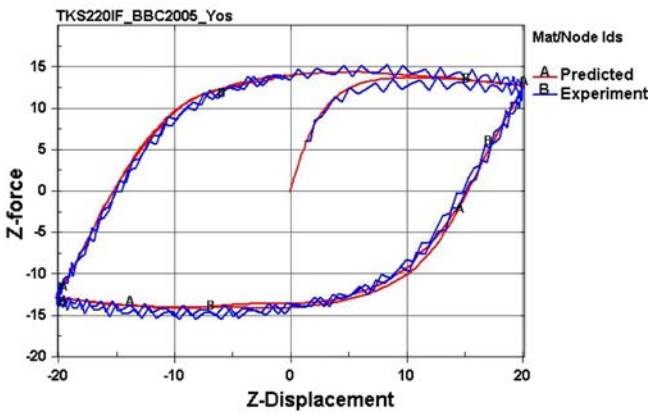

(e) Yoshida-Uemori hardening

Fig. 11 Fitting of simulated three-point bending tests to experimental results using the modified identification procedure and the five different hardening laws (two cycles). Material: TKS220IF

Acknowledgments The three-point bending tests were performed by Bertil Enqvist at Växjö University, Sweden. His contribution is gratefully acknowledged. The work has been performed within the Swedish National Research Program MERA (Manufacturing Engineering Research Area). Financial support has been provided by the Swedish Governmental Agency for Innovation Systems (Vinnova).

References

1. Yoshida F, Uemori T, Fujiwara K (2002) Elastic-plastic behavior of steel sheets under in-plane cyclic tension-compression at large strain. Int J Plast 18:633–659
2. Lee MG, Kim D, Kim C, Wenner ML, Wagoner RH, Chung K (2005) Spring-back evaluation of automotive sheets based on isotropic–kinematic hardening laws and non-quadratic anisotropic yield functions. Part II: characterization of material properties. Int J Plast 21:883–914
3. Balakrishnan V (1999) Measurements of in-plane Bauschinger effect in metal sheets. Master's thesis, The Ohio State University
4. Kuwabara T (2007) Advances in experiments on metal sheets and tubes in support of constitutive modeling and forming simulations. Int J Plast 23:385–419
5. Zhao KM, Lee JK (2001) Generation of cyclic stress–strain curves for sheet metals. J Eng Mater Technol 123:291–397
6. Omerspahic E, Mattiasson K, Enqvist B (2006) Identification of material hardening parameters by the three-point bending of metal sheets. Int J Mech Sci 48:1525–1532
7. Yoshida F, Urabe M, Toropov VV (1998) Identification of material parameters in constitutive model for sheet metals from cyclic bending tests. Int J Mech Sci 40:237–249
8. Carbonnière J, Thuillier S, Sabourin F, Brunet M, Manach PY (2009) Comparison of the work hardening of metallic sheets in bending-unbending and simple shear. Int J Mech Sci 51:122–130
9. Myers RH, Montgomery DC (1995) Response surface methodology. Wiley, New York
10. Carley KM, Kamneva NY, Reminga J (2004) Response surface methodology. CASOS Technical Report, Carnegie Mellon University, Pittsburgh
11. Stander N, Craig KJ, Müllerschön H, Reichert R (2005) Material identification in structural optimization using response surfaces. Struct Multidiscip Optim 29:93–102
12. (2007) LS-DYNA keyword user's manual, vol I, version 971. Livermore Software Technology Corporation (LSTC), Livermore
13. Stander N, Roux W, Eggleston T, Craig K (2007) LS-OPT user's manual, version 3.2. Livermore Software Technology Corporation (LSTC), Livermore
14. Hodge PG (1957) A new method of analyzing stresses and strains in work hardening solids. J Appl Mech 25:482–483
15. Crisfield MA (1997) More plasticity and other material non-linearity. In: Crisfield MA (ed) Non-linear finite element analysis of solid and structures, vol 2. Wiley, Chichester, pp 158–187
16. Armstrong PJ, Frederick CO (1966) A mathematical representation of the multiaxial Bauschinger effect. G.E.G.B Report RD/B/N. Berkeley Nuclear Laboratories, Central Electricity Generating Board, Berkeley, p 731
17. Geng L, Wagoner RH (2002) Role of plastic anisotropy and its evolution on springback. Int J Mech Sci 44:123–148
18. Yoshida F, Uemori T (2003) A model of large-strain cyclic plasticity and its application to springback simulation. Int J Mech Sci 45:1687–1702
19. Banabic D, Aretz H, Comsa DS, Parainou L (2005) An improved analytical description of orthotropy in metallic sheets. Int J Plast 21:493–512
20. Aretz H (2005) A non-quadratic plane yield function for orthotropic sheet metals. J Mater Process Technol 168:1–9
21. Eggertsen PA, Mattiasson K (2009) On the modeling of the bending-unbending behavior for accurate springback predictions. Int J Mech Sci 51:547–563
22. Kennedy JM, Belytschko T, Lin JI (1986) Recent developments in explicit Finite Element techniques and their applications to reactor structures. Nucl Eng Des 97:1–24